

Self-Supervised Deep Pose Corrections for Robust Visual Odometry

Brandon Wagstaff, Valentin Peretroukhin, and Jonathan Kelly

Abstract—We present a self-supervised deep pose correction (DPC) network that applies pose corrections to a visual odometry estimator to improve its accuracy. Instead of regressing inter-frame pose changes directly, we build on prior work that uses data-driven learning to regress pose corrections that account for systematic errors due to violations of modelling assumptions. Our self-supervised formulation removes any requirement for six-degrees-of-freedom ground truth and, in contrast to expectations, often improves overall navigation accuracy compared to a supervised approach. Through extensive experiments, we show that our self-supervised DPC network can significantly enhance the performance of classical monocular and stereo odometry estimators and substantially outperforms state-of-the-art learning-only approaches.

I. INTRODUCTION

Accurate self-localization is a prerequisite for reliable mobile autonomy and is especially important in situations where global navigation satellite system signals are unavailable or unreliable. Vision-based self-localization, in particular, has become ubiquitous since high-quality cameras are now relatively inexpensive and compact. Despite having a rich history in computer vision and robotics [1], visual localization still remains an open research topic, particularly in dynamic environments where many common modelling assumptions are violated [2].

At the heart of visual self-localization is visual odometry (VO): the process of estimating a camera’s own motion (or *egomotion*) from sequential image captures. To remain computationally tractable, ‘classical’ VO algorithms have typically assumed that the scene consists of static objects, has constant illumination, and lacks major occlusions. However, for long-term autonomy, it is critical for VO-based algorithms to maintain accuracy in spite of such adverse effects. Recently, in hopes of achieving robust pose estimates, end-to-end learning-based approaches have been proposed that completely replace classical techniques with learned models. By learning directly from data (using supervised [3] or self-supervised [4] methods), these network-based techniques have the potential to relax many of the assumptions that classical VO pipelines make, and as a result, to be robust to moving objects, poor illumination, and significant occlusions. However, to date, end-to-end-approaches have not surpassed the accuracy of classical VO algorithms.

Alternatively, other methods have augmented (rather than replaced) classical estimators with learned components. For example, learned measurement models have been used within

All authors are with the Space & Terrestrial Autonomous Robotic Systems (STARS) Laboratory at the University of Toronto Institute for Aerospace Studies (UTIAS), Toronto, Ontario, Canada, M3H 5T6. Email: <first name>.<last name>@robotics.utias.utoronto.ca

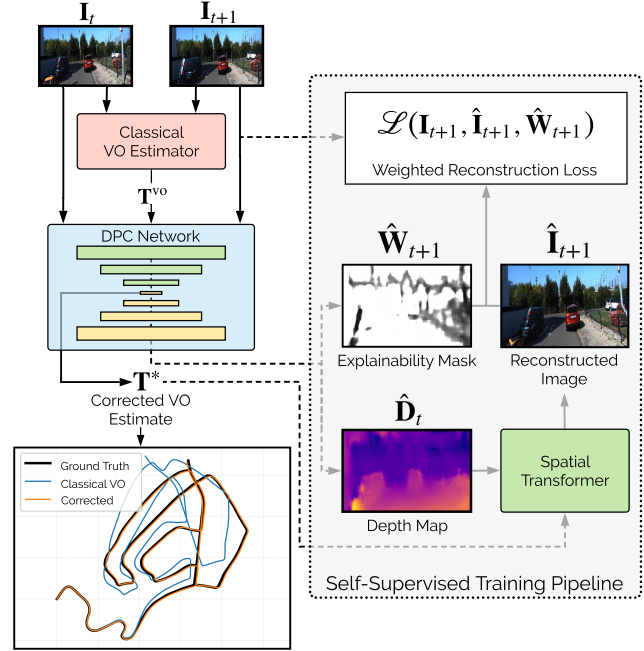


Fig. 1: Our self-supervised deep pose correction (DPC) network regresses a pose correction to a classical VO estimator.

Kalman filters [5] as a way to extract illumination direction from monocular images in an effort to reduce orientation drift [6], or as a way to more accurately initialize depth within a monocular VO pipeline [7]. By combining learning with classical pipelines, these methods aim to retain the interpretability and transferability of model-based techniques while leveraging the capacity and flexibility of data-driven model-free learning to improve accuracy and robustness.

Our approach, illustrated in Figure 1, follows in the spirit of these latter techniques. We fuse a classical VO pipeline with a data-driven model through the paradigm of learned pose *corrections*. Rather than training a network to regress the full inter-frame pose change from data alone, we instead rely on a classical VO estimate to produce a ‘large’ prior and use a deep neural network (DNN) to learn a smaller ‘correction’ that models how this classical estimator degrades in adverse situations (e.g., when there are many dynamic objects within the scene). We extend DPC-Net, the system proposed by [8], which introduced the paradigm of deep pose corrections (DPC) and used a DNN to predict corrections through a supervised training method driven by ground truth pose information. We improve upon this by replacing the supervised pose loss with a self-supervised photometric reconstruction loss that obviates the need for ground truth pose labels, which are often expensive or impractical to collect. Our loss formulation facilitates continual retraining

of the network when traversing new environments, since no supervision is required for training. In short, our novel contributions are:

- 1) a deep pose correction network that can be trained in a self-supervised manner, which obviates the need for ground truth pose labels,
- 2) substantial experimental validation of our method on the KITTI odometry dataset, showing that our method achieves state-of-the-art accuracy, and
- 3) the release of an open source implementation of our method in `PyTorch` [9].¹

II. BACKGROUND

Visual odometry is a well studied navigation technique that is used to estimate the robot’s six-degrees-of-freedom (DoF) pose change by solving for the camera’s egomotion between image frames. Typically, the inter-frame pose change is determined by optimizing for the pose that minimizes the error when aligning two sets of 3D points (for indirect methods) or pixels intensities (for direct methods) in a sequence of monocular or stereo camera images. Outlier rejection methods such as RANSAC [10] or robust losses are used to remove (or downweight) features (or pixels) that adversely affect the optimization process. By compounding relative pose changes, a global pose estimate is determined. However, VO is subject to superlinear error growth: in general, any small misestimate of the relative orientation change leads to larger and larger position errors. Typically, sources of error for VO include false correspondences (during feature matching), poor feature detection (due to camera motion blur or poor lighting), or the presence of dynamic objects within the scene. We refer the reader to [11] for a detailed and comprehensive review of visual odometry.

New data-driven paradigms for VO replace portions (or all) of the classical localization pipeline with a learned model. Some approaches [3] use supervised learning to train a convolutional neural network (CNN) to regress inter-frame pose changes in an end-to-end manner. Other techniques [12]–[14] rely on a self-supervised photometric reconstruction loss formulation for end-to-end VO. These methods train a network to regress the relative pose change between a current (source) view and a nearby (target) view by minimizing a photometric reconstruction loss. Such loss functions penalize the differences between the pixel intensities of the target image and the reconstructed image: under the assumptions that the scene is static, has constant illumination, and that there are no occlusions, the target image is reconstructed from the source image through an inverse compositional warping procedure that uses the predicted inter-frame pose change, a depth map (which is also learned) and the known camera intrinsic parameters. To train this type of network, a differentiable image warping tool called a spatial transformer [15] is applied to efficiently synthesize the reconstructed image; this allows gradients to be backpropagated from the reconstruction loss. Our work extends the self-supervised

pipeline to learn pose corrections, instead of full poses, based on a similar photometric loss.

Several others systems build on the baseline photometric reconstruction loss by imposing additional constraints. The authors of [16] use “composite transform constraints” to ensure that the predicted pose change across multiple frames is similar to the pose change produced by compounding the predicted pose changes between each individual image pair. In [13], epipolar geometry constraints are enforced to ensure that pixels from the source image are reprojected near to the epipolar line in the target image. The system in [4] uses a left-right stereo consistency loss that allows the depth network to output scaled depth maps from monocular camera images at test time. The approach described in [17] operates by learning to predict optical flow and disparity and then uses a classical RANSAC outlier rejection scheme to select a set of inlying pixels that can be used for pose estimation. The authors in [12] train a network to additionally regress an “explainability mask,” which ignores unreliable pixels that hinder image reconstruction, either because they break the photometric consistency assumption or because they correspond to objects that are moving. Our network relies on the explainability mask defined in [12].

III. APPROACH

Our approach (Figure 1) merges the self-supervised training procedure of end-to-end VO networks with the DPC framework of [6]. We replace the supervised loss of DPC-Net with a photometric reconstruction loss that does not require any external ground truth pose information, yet can still produce accurate pose corrections. Similar to other self-supervised methods, our network outputs a predicted inter-frame pose change and a depth map—however, our predicted inter-frame pose change is ‘initialized’ with an egomotion *prior* from a classical VO estimator. We compound this prior with a *correction* that is produced by our pose network. Using the depth map and the corrected inter-frame pose, we warp a source image into a target image and evaluate a photometric reconstruction loss. Unlike [6], which uses a supervised pose loss and thus requires SE(3) labels for training, our self-supervised photometric loss obviates the need for this type of 6-DoF ground truth, which can often be arduous to obtain.

Concretely, instead of directly estimating the inter-frame pose change, $\mathbf{T}_{t+1,t}$, our pose network aims to regress an SE(3) *correction*, $\mathbf{T}_{t+1,t}^{\text{corr}}$, that corrects a classical VO estimate, $\mathbf{T}_{t+1,t}^{\text{vo}}$,

$$\mathbf{T}_{t+1,t}^* = \mathbf{T}_{t+1,t}^{\text{corr}} \mathbf{T}_{t+1,t}^{\text{vo}}. \quad (1)$$

To parameterize this correction, we use an unconstrained vector from the $\mathfrak{se}(3)$ Lie algebra, $\boldsymbol{\xi}_{t+1,t}^{\text{corr}} \in \mathbb{R}^{6 \times 1}$, and then apply the (capitalized) exponential map to produce an on-manifold SE(3) correction:²

$$\mathbf{T}_{t+1,t}^{\text{corr}} = \text{Exp}(\boldsymbol{\xi}_{t+1,t}^{\text{corr}}). \quad (2)$$

²Our notation is based on and consistent with [18], [19], where a detailed review of matrix Lie groups is found.

¹See <https://github.com/utiasSTARS/ss-dpc-net>

Our network can be paired with any classical VO estimator and then trained to produce pose corrections specific to that estimator; inter-frame pose changes from the VO estimator are acquired for each pair of frames in the training dataset, and are then used to train the network to regress pose corrections that will minimize the photometric reconstruction loss. Herein, we train our system with a monocular and a stereo VO estimator (`libviso2-m` and `libviso2-s` [20], respectively) and show that our approach improves the localization accuracy of both estimators. We apply *monocular* corrections (our DPC network only takes as input images from a single camera) to `libviso2-m` and `libviso2-s`, as our loss formulation does not enforce any stereo image constraints; we leave this possibility as future work.

A. Image Warping Function

We apply an inverse compositional warping function that uses the source image’s estimated depth map, $\hat{\mathbf{D}}_t$, the camera intrinsics, and the (estimated) corrected pose change between frames. Assuming a pinhole camera model, image coordinates $\mathbf{u}_t = [u_t \ v_t]^T$ correspond to a 3D point $\mathbf{p}_t(\mathbf{u}_t) = [x_t \ y_t \ z_t]^T$ in the scene:

$$\mathbf{p}_t(\mathbf{u}_t) = \hat{\mathbf{D}}_t(\mathbf{u}_t) \begin{bmatrix} \frac{u_t - c_u}{f_u} & \frac{v_t - c_v}{f_v} & 1 \end{bmatrix}^T, \quad (3)$$

where (c_u, c_v) is the camera’s principal point, and (f_u, f_v) are the camera focal lengths in the horizontal and vertical directions, respectively. The estimated pose change between images is used to transform $\mathbf{p}_t(\mathbf{u}_t)$ to its 3D position at the next time-step,

$$\hat{\mathbf{p}}_{t+1}(\mathbf{u}_t) = \mathbf{T}_{t+1,t}^* \mathbf{p}_t(\mathbf{u}_t). \quad (4)$$

The 3D coordinates $\hat{\mathbf{p}}_{t+1}(\mathbf{u}_t)$ are reprojected onto the image plane according to

$$\begin{bmatrix} \hat{u}_{t+1} & 1 \end{bmatrix}^T = \begin{bmatrix} f_u & 0 & c_u \\ 0 & f_v & c_v \\ 0 & 0 & 1 \end{bmatrix} \frac{1}{\hat{z}_{t+1}} \hat{\mathbf{p}}_{t+1}(\mathbf{u}_t), \quad (5)$$

and the reconstructed target image is repopulated at the predicted pixel location with the original pixel intensity from the source image, $\hat{\mathbf{I}}_{t+1}(\hat{\mathbf{u}}_{t+1}) = \mathbf{I}_t(\mathbf{u}_t)$. Instead of reconstructing every pixel individually, we use a spatial transformer (*ST*) [15] to perform differentiable image warping, which efficiently reconstructs the entire target image from the source image:

$$\hat{\mathbf{I}}_{t+1} = ST(\mathbf{I}_t, \hat{\mathbf{D}}_t, \mathbf{T}_{t+1,t}^*, f_u, f_v, c_u, c_v). \quad (6)$$

B. Loss Function

We use a weighted photometric reconstruction loss, which compares the reconstructed image with the target image. For a dataset with N training examples (each consisting of a source and target image of dimension $H \times W$ with C colour

channels), we define our loss function as:³

$$\mathcal{L} = \frac{1}{NCHW} \sum_{n=1}^N \sum_{u,v} (\mathcal{L}_{\text{phot}} + \lambda_{\text{exp}} \mathcal{L}_{\text{exp}} + \lambda_{\text{rot}} \mathcal{L}_{\text{rot}}). \quad (7)$$

We now describe each of the three terms of this loss in detail. The first term, the pixel-wise weighted photometric reconstruction loss, compares a pixel (u, v) from the target image with the corresponding pixel from the reconstructed image:

$$\mathcal{L}_{\text{phot}} = \hat{\mathbf{W}}_{t+1}(u, v) \left| \hat{\mathbf{I}}_{t+1}(u, v) - \mathbf{I}_{t+1}(u, v) \right|. \quad (8)$$

Each pixel loss is weighted by the explainability mask, $\hat{\mathbf{W}}_{t+1}(u, v) \in (0, 1)$, which accounts for situations in which the photometric consistency approximation is violated (e.g., due to lighting changes, dynamic objects, or occlusions). A high quality image reconstruction generally implies that the network’s depth and pose correction estimates are also of high quality. To prevent the trivial solution of setting all explainability weights to zero, we use a regularization term, \mathcal{L}_{exp} , that is a cross-entropy loss with a constant label 1 for each pixel,

$$\mathcal{L}_{\text{exp}} = -\log \hat{\mathbf{W}}_{t+1}(u, v). \quad (9)$$

Figure 2b illustrates an example scene where this mask is especially useful for mitigating the effects of moving objects.

Lastly, \mathcal{L}_{rot} is a loss term for training samples that incorporate large rotations; since these samples are less common than samples with smaller rotations, but are significantly more important for egomotion estimation, we use this loss to increase their relative weight compared to other samples. The loss term \mathcal{L}_{rot} is the same as the photometric reconstruction term, but is set to zero for all samples except those with large rotations (according to the classical estimator’s orientation estimate, \mathbf{R}_{vo}):

$$\mathcal{L}_{\text{rot}} = \begin{cases} 0 & \|\log(\mathbf{R}_{\text{vo}})^\vee\| < \gamma \\ \mathcal{L}_{\text{phot}} & \|\log(\mathbf{R}_{\text{vo}})^\vee\| \geq \gamma \end{cases} \quad (10)$$

C. Model Architecture

Our network jointly estimates the pose correction, depth prediction, and explainability mask. Figure 2a provides a graphical illustration of the network structure, which is a modified version of the network in [12] that used a U-Net encoder-decoder [21]. The network inputs are two images (the source and the target image) concatenated with the optical flow vectors estimated between the two images. The optical flow vectors, generated using the Gunnar-Farneback algorithm [22], are incorporated because it has been shown in [23] that using intermediate representations adds explicit knowledge to the network that can improve performance

³Note that while many similar implementations use a multi-scale loss, we found that a multi-scale loss was detrimental to the quality of our pose corrections; we suspect this is the case because the regressed pose corrections are very small quantities, which require a high image resolution to learn.

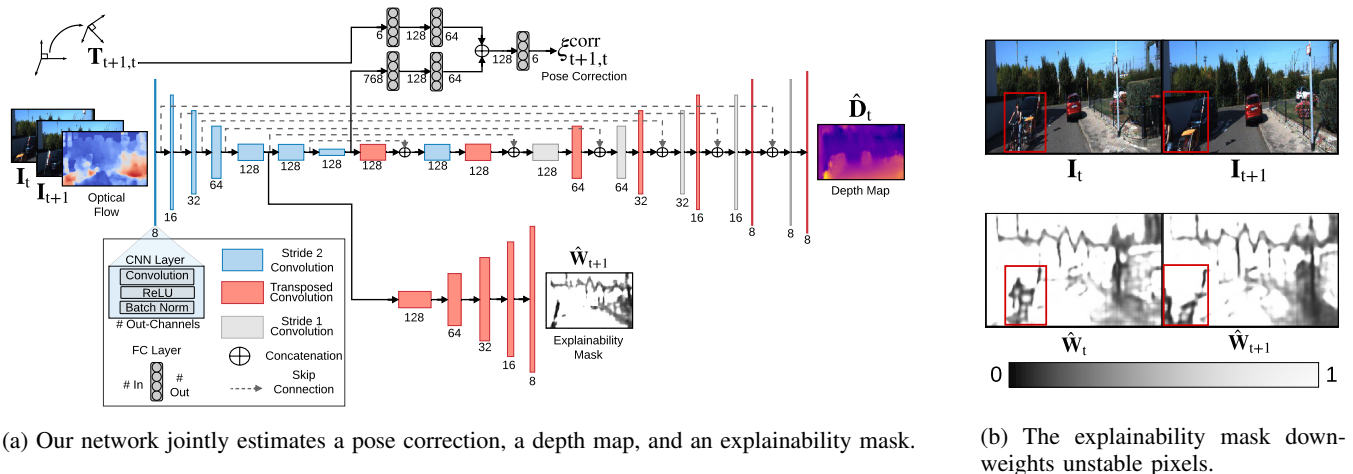


Fig. 2: A network diagram of our self-supervised DPC network and an example of where its explainability mask is useful.

on vision-based tasks. Additionally, we provide the network with the classical VO estimate (parameterized as a 6×1 Lie algebra vector through the logarithmic map), which is concatenated with the fully-connected layers near the centre of the network. Notably, we depart from prior work by unifying the depth and pose networks into a single network, which significantly improves the ability to generalize beyond the training data; incorporating the optical flow and the `libviso2` pose estimates as inputs additionally improved the results.

The encoder network is composed of five blocks (in blue); each consists of a (stride 2) 2D convolution layer, a ReLU activation, and a batch normalization layer. We avoid the use of pooling layers, as they lead to spatial invariance, which would be detrimental for visual localization tasks. At the bottleneck, we branch the network into depth, explainability mask, and pose correction subnetworks. For the depth and explainability mask, we upsample from the bottleneck using decoder blocks which consist of a 2D transposed convolution layer [24] followed by a ReLU activation. Our depth prediction layer is a 2D (stride 1) convolution that reduces the channel layer to one, and a ReLU activation which ensures the output is positive.⁴ The final explainability mask layer is a sigmoid activation, which compresses the pixel values to lie within $(0, 1)$.

IV. EXPERIMENTS

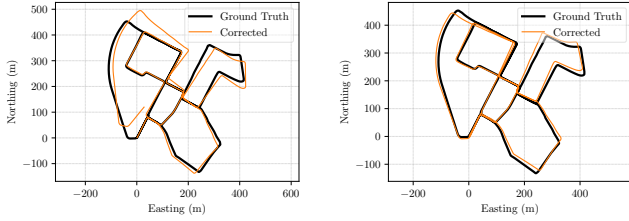
To train, validate, and test our system, we used the KITTI odometry dataset [25], [26]. Our full dataset consisted of colour images from the odometry sequences 00, 02, 05-10, and an additional 24 training sequences (approximately 10,000 images) from the “city”, “residential”, and “road”

⁴In practice, we output the inverse depth estimate (to avoid regressing to infinite depths), and invert the network output to produce a depth estimate. Our network actually outputs a depth prediction at each of the final convolutional layers; each prediction is concatenated with the next layer (e.g., the prediction from the fourth-last layer is concatenated with its other output channels prior to being passed to the third-last layer). For interpretability, we omitted this from the network diagram.

categories of the raw KITTI dataset. The images were preprocessed to be more amenable for training: they were resized to 240×376 pixels and whitened using the ImageNet [27] statistics. Furthermore, similar to keyframe-based approaches, we used the classical VO estimates to filter out frames from the sequence that had little motion by removing those frames whose inter-frame translation or rotation was less than 1.5 m or 0.4° , respectively. For all of the sequences, we estimated the camera poses using the `libviso2` package [20], which is a popular classical VO estimator (and, for consistency, is the same estimator used in DPC-Net [8]). We generated monocular (`libviso2-m`) and stereo (`libviso2-s`) egomotion estimates; these estimates are included in our open source repository.

DPC models were trained for both the monocular and stereo `libviso2` estimators. We trained the DPC networks for up to 30 epochs with the Adam optimizer [28] (with minibatch sizes of 32) using an initial learning rate of 1×10^{-3} and 5×10^{-5} for the stereo and monocular DPC models, respectively. We reduced the learning rate by a factor of 0.5 every ten and four epochs for the monocular and stereo DPC models, respectively. We used dropout ($p = 0.5$) for all of the fully connected layers with a weight decay coefficient of 4×10^{-6} . All other hyperparameters were held constant during training. In our loss function (Equation (7)), we selected the hyperparameter $\lambda_{\text{exp}} = 0.23$ to cause the explainability mask to typically regress values close to one; progressively larger weights caused the explainability mask outputs to uniformly decrease, rather than decreasing only for unreliable pixels. We selected $\lambda_{\text{rot}} = 4$ and $\gamma = 0.005$ in order to emphasize larger rotations in the cost function. Using leave-one-out cross-validation, we trained a unique model for each test sequence, while using a single sequence for validation and all other sequences for training.

The primary challenge during training was selecting the training epoch whose model parameters produced high quality pose corrections; since no ground truth pose information



(a) Epoch 5: 40 loop closures detected. (b) Epoch 28: 122 loop closures detected.

Fig. 3: Loop closure comparison for test sequence (00): compared to ground truth, the epoch with a higher number of detected loop closures resulted in a more accurate trajectory estimate.

was used in the training procedure, the network learned to minimize the photometric reconstruction error, not the localization error. Consequently, although the training procedure generally resulted in high-accuracy pose corrections, there were epochs that resulted in a low validation loss, but not in high-quality pose corrections. To address this, we developed two criteria to identify the training epoch with the most accurate pose corrections—both are evaluated in Section V.

Gradient Criterion: First, we recompute the photometric loss *only* for pixels with large gradient values (since the photometric errors for these pixels are highly sensitive to an erroneous pose correction). To compute the gradient loss, we generate a gradient mask by filtering out all pixels whose gradient value is below a constant, γ_{grad} :

$$\frac{|\nabla_x \mathbf{I}(x, y)| + |\nabla_y \mathbf{I}(x, y)|}{2} \leq \gamma_{\text{grad}}. \quad (11)$$

Empirically, we found that the gradient loss is more effective for identifying the epoch with the highest performing model than the loss from Equation (7).

Loop Closure Criterion: Second, we note that we can relate the number of loop closures in the compounded validation trajectory with the accuracy of the pose corrections in the test set (see Figure 3). To identify loop closures in the validation trajectory, we use predefined thresholds⁵ and save the model at the training epoch that produces the most loop closures for the validation set. We emphasize that although this method does require the *validation sequence* to have loop closures (which we ensured herein by selecting the KITTI validation sequences 00 and 05 that consist of multiple traverses of the same road) it places no such restriction on the *test sequence*. Therefore, as long as one can find a validation sequence that has multiple traverses of the same path, this epoch selection criterion can be applied.

V. RESULTS

Our evaluation metrics were the mean absolute trajectory error (m-ATE) and the mean segment error (m-SE). In accordance with the KITTI odometry benchmark, we computed the mean error for all segments that were

⁵For a given pose, $\mathbf{T}_{t,0}$, we defined a loop closure event at time $t+n$ if the pose $\mathbf{T}_{t+n,0}$ was within 7 m and 8.5° of the pose at time t . We also ensured that the forward translation of $\mathbf{T}_{t+n,t}$ exceeded 10 m to ensure that the vehicle was performing a second traverse along the same path.

TABLE I: Results of correcting `libviso2-m` with our DPC network. We benchmark against several state-of-the-art learning-based monocular VO estimators.

Estimator	Stopping Criterion	Mean Segment Error			
		Seq. 09		Seq. 10	
		Trans. (%)	Rot. ($^\circ/100\text{m}$)	Trans. (%)	Rot. ($^\circ/100\text{m}$)
<code>libviso2-m</code>		8.66	2.76	8.00	3.32
SfMLearner [12]	—	18.8	3.21	14.3	3.30
UnDeepVO [4]	—	7.01	3.61	10.6	4.65
Zhan et al. [29]	—	11.9	3.60	12.6	4.65
Zhu et al. [17]	—	4.66	1.69	6.30	1.59
Luo et al. [30]	—	3.72	1.60	6.06	2.22
Ours ¹	<i>Gradient Loss</i>	2.82	0.76	3.81	1.34
	<i>Loop Closure</i>	2.13	0.80	3.48	1.38

¹ Validation sequence 05 for sequence 09, and 00 for sequence 10.

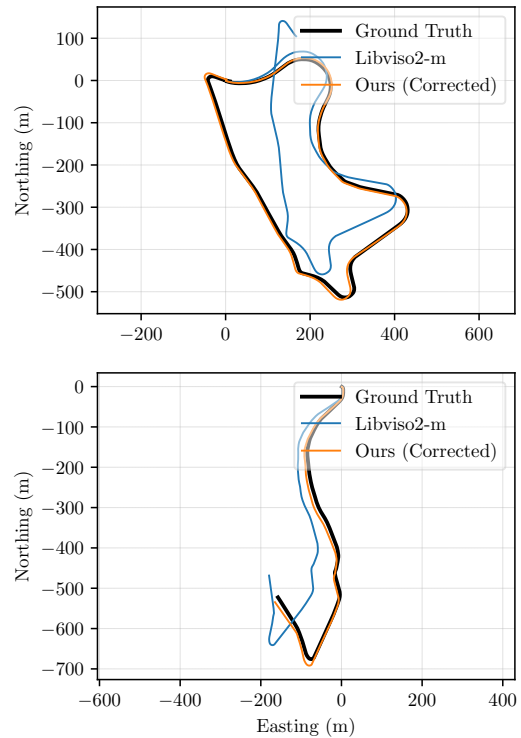


Fig. 4: Corrected `libviso2-m` estimates for sequences 09 (top) and 10 (bottom). We show the original `libviso2-m` estimate.

{100, 200, ..., 800} metres in length; we report the overall average herein.

Monocular Results: We applied corrections to the `libviso2-m` estimates and compared the corrected trajectories with state-of-the-art end-to-end monocular VO estimators. Prior to applying corrections, we rescaled the `libviso2-m` estimate to be consistent with ground truth by adjusting each relative pose change to match the ground truth inter-frame displacement (while this is not fully self-supervised, this is in line with how other monocular VO systems [12], [29] are evaluated). Table I shows the mean segment errors for test sequences 09 and 10 of the KITTI dataset, which are the most common test sequences for monocular methods; notably, we achieve state-of-the-art accuracies compared to modern learning-based techniques. Fig-

TABLE II: Results of correcting libviso2-s with our self-supervised DPC network.

Test Sequence (Length)	Estimator	Stopping Criterion	m-ATE		m-SE	
			Trans. (m)	Rot. ($^{\circ}$)	Trans. (%)	Rot. ($^{\circ}$ /100m)
00 (3.7 km)	libviso2-s	—	53.77	13.30	2.79	1.292
	libviso2-s + DPC-Net [8]	—	15.68	3.07	1.62	0.559
	Direct Keyframe	—	12.41	2.45	1.28	0.542
	Ours ¹	<i>Gradient Loss</i>	12.59	2.47	0.99	0.457
		<i>Loop Closure</i>	14.65	3.32	1.03	0.444
02 (5.1 km)	libviso2-s	—	68.60	12.55	2.42	0.923
	libviso2-s + DPC-Net	—	17.69	2.86	1.16	0.436
	Direct Keyframe	—	16.33	3.19	1.21	0.467
	Ours ¹	<i>Gradient Loss</i>	15.69	3.52	1.11	0.499
		<i>Loop Closure</i>	21.31	1.91	0.83	0.373
05 (2.2 km)	libviso2-s	—	19.68	6.30	2.31	1.135
	libviso2-s + DPC-Net	—	9.82	3.57	1.34	0.562
	Direct Keyframe	—	5.83	2.05	0.69	0.320
	Ours ²	<i>Gradient Loss</i>	10.92	4.10	1.33	0.597
		<i>Loop Closure</i>	4.03	1.18	0.83	0.304

¹ Validation sequence 05. ² Validation sequence 00.

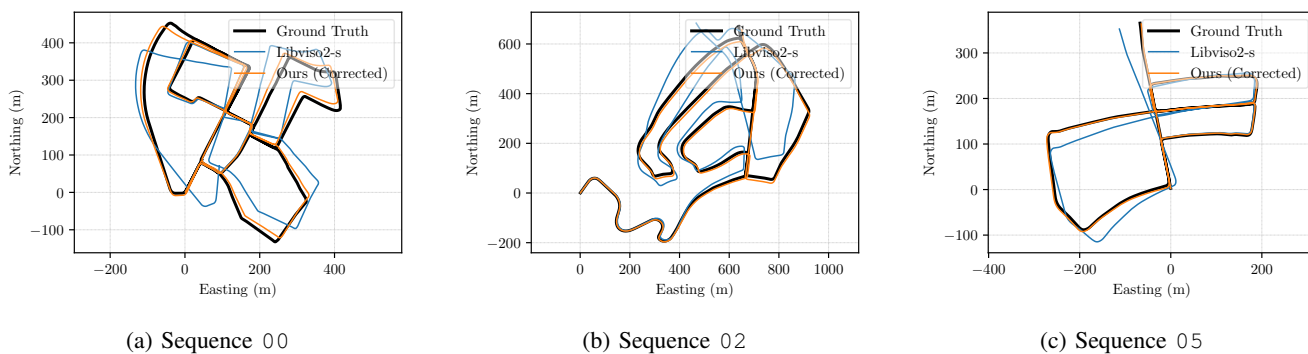


Fig. 5: Corrected libviso2-s trajectories. We show the original libviso2-s estimate for comparison.

ure 4 illustrates the corrected trajectories, which appear to be significantly more accurate than the original libviso2-m estimate.

Stereo Results: We applied corrections to libviso2-s and compared the corrected trajectories with the corrected trajectories from DPC-Net [8]. In practice, we found that only rotation (SO(3)) corrections were required to adjust the libviso2-s estimates, since the translation estimates were already highly accurate. Our DPC network uses monocular images only to regress pose corrections and so cannot provide any improvement by correcting the translation estimates. We evaluated our DPC network on test sequences 00, 02, 05. Table II lists the m-ATE and m-SE for our corrected trajectories, while Figure 5 visually depicts these results and compares them to the libviso2-s estimates. We benchmark against DPC-Net [8] and also a direct, keyframe-based VO implementation based on DSO [31]. Both of our proposed modes of operation are consistently more accurate than these competing methods for the three test sequences.

VI. CONCLUSIONS AND FUTURE WORK

In this paper, we presented a deep network that is trained to correct classical VO estimators in a self-supervised manner,

without the need for 6-DoF ground truth. By regressing pose corrections (instead of the full inter-frame pose change), our approach produces trajectory estimates that are significantly more accurate than existing state-of-the-art end-to-end VO networks. We attribute this increase in accuracy to the union of learning-based and classical (handcrafted) models. Our method preserves the core geometric framework that generally yield accurate egomotion estimates under nominal conditions, and pairs it with a learning approach that applies corrections when modelling assumptions are violated or other confounding factors are present. Our self-supervised loss formulation facilitates continual model retraining with new data. As future work, we plan to incorporate stereo constraints (e.g., the left-right consistency constraint of [4]) or other sources of metric information (e.g., inertial measurement unit data) to better improve our translation corrections.

ACKNOWLEDGMENTS

This work was supported in part by the Natural Sciences and Engineering Research Council (NSERC) of Canada. We gratefully acknowledge the contribution of NVIDIA Corporation, who provided the Titan X GPU used for this research through their Hardware Grant Program.

REFERENCES

- [1] M. Aqel, M. Marhaban, M. Saripan, and N. Ismail, "Review of visual odometry: types, approaches, challenges, and applications," *SpringerPlus*, vol. 5, no. 1, p. 1897, 2016.
- [2] Cadena, C. and Carlone, L. and Carrillo, H. and Latif, Y. and Scaramuzza, D. and Neira, J. and Reid, I. and Leonard, J., "Past, present, and future of simultaneous localization and mapping: Toward the robust-perception age," *IEEE Trans. Robot.*, vol. 32, no. 6, pp. 1309–1332, 2016.
- [3] S. Wang, R. Clark, H. Wen, and N. Trigoni, "DeepVO: Towards end-to-end visual odometry with deep recurrent convolutional neural networks," in *Proc. IEEE Int. Conf. Robot. Autom. (ICRA)*, 2017, pp. 2043–2050.
- [4] R. Li, S. Wang, Z. Long, and D. Gu, "UnDeepVO: Monocular visual odometry through unsupervised deep learning," in *Proc. IEEE Int. Conf. Robot. Autom. (ICRA)*, 2018, pp. 7286–7291.
- [5] T. Haarnoja, A. Ajay, S. Levine, and P. Abbeel, "Backprop KF: Learning discriminative deterministic state estimators," in *Proc. Conf. Neural Inf. Process. Syst. (NeurIPS)*, 2016, pp. 4376–4384.
- [6] V. Peretroukhin, L. Clement, and J. Kelly, "Reducing drift in visual odometry by inferring sun direction using a bayesian convolutional neural network," in *Proc. IEEE Int. Conf. Robot. Autom. (ICRA)*, 2017, pp. 2035–2042.
- [7] N. Yang, R. Wang, J. Stückler, and D. Cremers, "Deep virtual stereo odometry: Leveraging deep depth prediction for monocular direct sparse odometry," in *Proc. Eur. Conf. Comput. Vision (ECCV)*, 2018.
- [8] V. Peretroukhin and J. Kelly, "DPC-Net: Deep pose correction for visual localization," *IEEE Robot. Autom. Lett.*, vol. 3, no. 3, pp. 2424–2431, 2018.
- [9] A. Paszke, S. Gross, S. Chintala, G. Chanan, E. Yang, Z. DeVito, Z. Lin, A. Desmaison, L. Antiga, and A. Lerer, "Automatic differentiation in PyTorch," in *Workshop on Automatic Differentiation, Conf. Neural Inf. Process. Syst. (NeurIPS)*, 2017.
- [10] M. Fischler and R. Bolles, "Random sample consensus: A paradigm for model fitting with applications to image analysis and automated cartography," *J. Commun. ACM*, vol. 24, no. 6, pp. 381–395, 1981.
- [11] D. Scaramuzza and F. Fraundorfer, "Visual odometry [tutorial]," *IEEE Robot. Autom. Mag.*, vol. 18, pp. 80–92, 2011.
- [12] T. Zhou, M. Brown, N. Snavely, and D. Lowe, "Unsupervised learning of depth and ego-motion from video," in *Proc. IEEE Conf. Comput. Vision Pattern Recognition (CVPR)*, 2017, pp. 1851–1858.
- [13] V. Prasad and B. Bhowmick, "SfMLearner++: Learning monocular depth & ego-motion using meaningful geometric constraints," in *Proc. IEEE Winter Conf. Appl. Comput. Vision (WACV)*, 2019, pp. 2087–2096.
- [14] S. Vijayanarasimhan, S. Ricco, C. Schmid, R. Sukthankar, and K. Fragkiadaki, "SfM-Net: Learning of structure and motion from video," *arXiv preprint arXiv:1704.07804*, 2017.
- [15] M. Jaderberg, K. Simonyan, A. Zisserman, and K. Kavukcuoglu, "Spatial transformer networks," in *Proc. Conf. Neural Inf. Process. Syst. (NeurIPS)*, 2015, pp. 2017–2025.
- [16] G. Iyer, J. Murthy, G. Gupta, K. Krishna, and L. Paull, "Geometric consistency for self-supervised end-to-end visual odometry," in *Proc. IEEE Conf. Comput. Vision Pattern Recognition Workshops*, 2018, pp. 267–275.
- [17] A. Zhu, W. Liu, Z. Wang, V. Kumar, and K. Daniilidis, "Robustness meets deep learning: An end-to-end hybrid pipeline for unsupervised learning of egomotion," *arXiv preprint arXiv:1812.08351*, 2018.
- [18] T. Barfoot, *State Estimation for Robotics*, 1st ed. New York, NY, USA: Cambridge University Press, 2017.
- [19] J. Solà, J. Deray, and D. Atchuthan, "A micro lie theory for state estimation in robotics," *arXiv preprint arXiv:1812.01537*, 2018.
- [20] A. Geiger, J. Ziegler, and C. Stiller, "Stereoscan: Dense 3D reconstruction in real-time," in *Proc. IEEE Intell. Veh. Symp. (IV)*, 2011, pp. 963–968.
- [21] Ronneberger, O. and Fischer, P. and Brox, T., "U-Net: Convolutional networks for biomedical image segmentation," in *Proc. Int. Conf. Medical Image Computing Computer-Assisted Intervention*. Springer, 2015, pp. 234–241.
- [22] G. Farnebäck, "Two-frame motion estimation based on polynomial expansion," in *Proc. Scandinavian Conf. Image Analysis*, 2003, pp. 363–370.
- [23] B. Zhou, P. Krähenbühl, and V. Koltun, "Does computer vision matter for action?" *Sci. Robot.*, vol. 4, no. 30, 2019.
- [24] V. Dumoulin and F. Visin, "A guide to convolution arithmetic for deep learning," *arXiv preprint arXiv:1603.07285*, 2016.
- [25] A. Geiger, P. Lenz, and R. Urtasun, "Are we ready for autonomous driving? the KITTI vision benchmark suite," in *Proc. IEEE Conf. Comput. Vision Pattern Recognition (CVPR)*, 2012, pp. 3354–3361.
- [26] A. Geiger, P. Lenz, C. Stiller, and R. Urtasun, "Vision meets robotics: The KITTI dataset," *Int. J. Robot. Res. (IJRR)*, vol. 32, no. 11, pp. 1231–1237, 2013.
- [27] J. Deng, W. Dong, R. Socher, L. Li, K. Li, and L. Fei-Fei, "ImageNet: A large-scale hierarchical image database," in *Proc. IEEE Conf. Comput. Vision Pattern Recognition (CVPR)*, 2009, pp. 248–255.
- [28] D. P. Kingma and J. Ba, "Adam: A method for stochastic optimization," *arXiv preprint arXiv:1412.6980*, 2014.
- [29] H. Zhan, R. Garg, C. Weerasekera, K. Li, H. Agarwal, and I. Reid, "Unsupervised learning of monocular depth estimation and visual odometry with deep feature reconstruction," in *Proc. IEEE Conf. Comput. Vision Pattern Recognition (CVPR)*, 2018, pp. 340–349.
- [30] C. Luo, Z. Yang, P. Wang, Y. Wang, W. Xu, R. Nevatia, and A. Yuille, "Every pixel counts++: Joint learning of geometry and motion with 3d holistic understanding," *arXiv preprint arXiv:1810.06125*, 2018.
- [31] J. Engel, V. Koltun, and D. Cremers, "Direct sparse odometry," *IEEE Trans. Pattern Anal. Machine Intell.*, vol. 40, no. 3, pp. 611–625, 2017.